ORIGINAL RESEARCH

Activation of the Integrated Stress Response and Metabolic Dysfunction in a Murine Model of Sleep Apnea

Abdelnaby Khalyfa[1], Zhuanhong Qiao[1], Alex Gileles-Hillel[1], Ahamed A. Khalyfa[1], Mahzad Akbarpour[1], Brian Popko[2], and David Gozal[1]

[1]Section of Pediatric Sleep Medicine, Department of Pediatrics, and [2]Department of Neurology, Pritzker School of Medicine, Biological Sciences Division, The University of Chicago, Chicago, Illinois

ORCID ID: 0000-0001-8195-6036 (D.G.).

Abstract

Intermittent hypoxia (IH) induces activation of the integrated stress response (ISR), but its role in IH-induced visceral white adipose tissue (vWAT) insulin resistance is unknown. CHOP is activated by chronic ISR, whereas GADD34 dephosphorylates the subunit of translation initiation factor 2 (eIF2α), leading to termination of the ISR. We hypothesized that CHOP/Gadd34 null mice would not manifest evidence of insulin resistance after IH exposures. Eight-week-old CHOP/GADD34$^{-/-}$ (double mutant [DM]) and wild-type (WT) littermates were randomly assigned to IH or room air (RA) exposures for 6 weeks. Glucose and insulin tolerance tests were performed, and regulatory T cells (Tregs) and macrophages in vWAT were assessed. Phosphorylated eIF2α:total eIF2α, ATF4, XBP1 expression, and insulin-induced pAKT/AKT expression changes were examined in vWATs. Single GADD34$^{-/-}$ and PERK$^{+/-}$ mice were also evaluated. Body weight and vWAT mass were reduced in DM and WT mice after IH. M1/M2 macrophages and inflammatory macrophages (Ly-6c^{high}) were significantly increased in WT vWAT but remained unchanged in DM mice. Tregs were significantly decreased in WT vWAT but not in DM mice. Systemic insulin and glucose tolerance tests revealed insulin resistance in IH-WT but not in IH-DM mice. Similarly, decreased pAKT/AKT responses to exogenous insulin emerged in IH-WT compared with RA-WT mice, whereas no significant differences emerged in IH-DM compared with DM-RA. Chronic ISR activation appears to contribute to the insulin resistance and vWAT inflammation that characteristically emerge after long-term IH exposures in a murine model of obstructive sleep apnea.

Keywords: intermittent hypoxia; integrated stress response; obstructive sleep apnea; double-mutant GADD34/CHOP; PERK

Clinical Relevance

Hypoxia activates the integrated stress response (ISR), and intermittent hypoxia induces metabolic dysfunction both systemically and in visceral adipose tissues. The role of the ISR in metabolic dysfunction in sleep apnea is unknown. We show that the ISR may play a significant role in visceral adipose tissue inflammation and metabolic dysfunction in the context of sleep apnea.

The endoplasmic reticulum (ER) is a key intracellular organelle that mediates protein translocation, folding, and post-translational modifications. Perturbations in ER function, a process commonly termed "ER stress," trigger the unfolded protein response (UPR), and this UPR highly coordinated set of intracellular signal transduction events that are designed to preserve or restore protein homeostasis is usually denominated the integrated stress response (ISR) (1). The ISR characteristically involves the activation of three signaling proteins: IRE1α (inositol-requiring protein-1α), PERK (protein

(Received in original form February 12, 2017; accepted in final form May 10, 2017)

This work was supported by National Institutes of Health grant NS034939 (B.P.) and the Herbert T. Abelson Chair (D.G.).

Author Contributions: A.K. performed experiments, analyzed data, and drafted the initial version of the manuscript. Z.Q., A.G.-H., A.A.K., and M.A. performed experiments and analyzed data. B.P. provided transgenic mice and contributed to data interpretation. D.G. provided the conceptual framework for the project, supervised experiments, analyzed data, and edited the manuscript. All authors reviewed and approved the final version of the manuscript. D.G. serves as the guarantor of the paper and takes responsibility for the integrity of the work as a whole, from inception to published article.

Correspondence and requests for reprints should be addressed to David Gozal, M.D., M.B.A., Department of Pediatrics, Pritzker School of Medicine, Biological Sciences Division, The University of Chicago, KCBD, Room 4100, 900 E. 57th Street, Mailbox 4, Chicago, IL 60637. E-mail: dgozal@uchicago.edu

This article has a data supplement, which is accessible from this issue's table of contents at www.atsjournals.org

Am J Respir Cell Mol Biol Vol 57, Iss 4, pp 477–486, Oct 2017

Originally Published in Press as DOI: 10.1165/rcmb.2017-0057OC on June 8, 2017
Internet address: www.atsjournals.org

kinase RNA [PKR]-like ER kinase), and ATF6 (activating transcription factor 6). Accumulation of unfolded proteins in the ER fosters IRE1α oligomerization and autophosphorylation of IRE1α, which ultimately increase the splicing of XBP-1 (X box-binding protein-1) mRNA and allow for synthesis of the XBP-1 protein. PERK-induced phosphorylation of eIF2α also permits the preferential translation of UPR-dependent genes, such as ATF4 (activating transcriptional factor 4), which then regulate CHOP (transcriptional factor C/EBP homologous protein) and GADD34 (growth arrest and DNA damage-inducible-34) expression and activity. In the context of ER stress, ATF6 is a transcriptional factor that will translocate to the Golgi compartment, where it is cleaved by two proteases: S1P (serine protease site-1) and S2P (metalloprotease site-2 protease). The cleaved N-terminal cytosolic domain of ATF6 then translocates to the nucleus to bind the ATF/cAMP response elements (CRE) and ER stress–response elements (ERSE-1), leading to the activation of important target genes such as BiP, Grp94, and CHOP. Thus, chronic ISR activation leads to downstream ATF4 and CHOP activation, whereas GADD34 dephosphorylates eIF2α, leading to termination of the protective early-phase component of the ISR.

Chronic and highly prevalent disorders such as obstructive sleep apnea (OSA) have been associated with the presence of metabolic dysfunction in general, and more particularly with the presence of insulin resistance and dyslipidemia (2–4). Recent work from our laboratory and others has suggested that sleep fragmentation (SF) and intermittent hypoxia (IH) during sleep, the major constitutive elements of OSA, serve as major determinants of visceral white adipose tissue (vWAT) insulin resistance by inducing local inflammatory changes involving polarization of adipose tissue macrophages (5–7). In parallel with these findings, both IH and SF have been shown to induce the ISR in several target organs associated with OSA-induced morbidities (8, 9). It is now quite well established that the ISR plays an important role in the capacity of cells to deal with nutrient fluctuations, and additionally that some nutrients, such as saturated fats, induce the ISR. For example, a high-fat diet will chronically induce the ISR in both adipose tissues and liver, and chronic ISR activation is mechanistically associated with evidence of insulin resistance and metabolic dysfunction (10). Thus, based on the aforementioned observations, we hypothesized that IH-induced metabolic perturbations in a murine model of OSA would be mediated, at least in part, by prolonged and sustained activation of the ISR.

Materials and Methods

Animals

All experiments were approved by The University of Chicago Institutional Animal Care and Use Committee (IACUC protocol #72169). CHOP and GADD34 double-mutant (DM) mice were generated by crossing single mutants initially created in David Ron's laboratory (http://ron.cimr.cam.ac.uk/RONMICE_JAX.html) (11, 12) to produce mice that were heterozygous for both mutations. Double heterozygotes were then interbred to generate the homozygous DMs on a C57BL/6J background. We also used double-stranded RNA-activated $PERK^{-/+}$ mice (13) and $GADD34^{-/-}$ (11) knockout mice, with both strains originating from Dr. David Ron's laboratory. The animals were fed a normal chow diet and housed in a controlled environment with 12-hour light/dark cycles (7:00 A.M. to 7:00 P.M.) at constant temperature (24 ± 0.2°C) with *ad libitum* access to food and water. For all experiments, the authors who performed the experiment were blinded to the identity of the mice being tested.

IH Exposures

Mice were exposed to IH as previously described (14). Briefly, mice were subjected for 12 hours during daylight to IH/normoxia cycles of 3 minutes duration (hypoxia, nadir of fractional inspired oxygen concentration [$F_{I_{O_2}}$]: 6.4% for 90 s alternating with normoxia [$F_{I_{O_2}}$, 21%] for 90 s) for 6 weeks. This IH profile is associated with a reproducible nadir of oxyhemoglobin saturations in the 65–72% range. Normoxic ($F_{I_{O_2}}$ 21%) conditions were used during the 12-hour lights-off period. Control animals were exposed to circulating room air (RA; $F_{I_{O_2}}$ 21%) during daylight and the lights-off period. Programmed gas concentrations were circulated into each chamber, and an internal O_2 analyzer measured the O_2 concentration continuously. Deviations from the fixed concentrations were automatically corrected by a computerized system of solenoid valves controlling gas outlets that added either N_2 or O_2 from adjoining connected reservoirs. Ambient CO_2 in the chamber was maintained at less than 0.01%, and humidity was also maintained at 40–50% by circulating the gas through a freezer and silica gel. The mice were divided into three groups (DM [$CHOP^{-/-}$/$GADD34^{-/-}$], $PERK^{-/+}$, and $GADD34^{-/-}$), and each group was exposed to IH and RA for 6 weeks with the corresponding wild-type (WT) controls.

Glucose Tolerance Test and Insulin Assay

Intraperitoneal glucose tolerance tests (GTTs) were performed at the end of the 6-week exposures. After 3 hours of fasting, DM mice were injected with glucose (2 mg/g body weight intraperitoneally). Water was provided ad lib during the fasting period. Blood samples were collected from the tail vein in heparin-coated capillary tubes for glucose determination at 0, 4, 15, 30, 60, 90, and 120 minutes. Blood glucose was measured using a OneTouch Ultra2 glucometer (LifeScan, Milpitas, CA). Glucose responses during the GTTs were evaluated by estimating the total area under the glycemic responses versus time. Blood samples for insulin determination were also obtained from the cut tip of the tail at the same aforementioned time points after glucose injection. Plasma insulin assays were performed with ELISA kits (EMD Millipore, Billerica, MA) according to the manufacturer's protocol. The appropriate range for the insulin assay was 0.2–10 ng/ml, with a limit of sensitivity of 0.2 ng/ml and intra- and interassay variations of 3.73% and 10.52%, respectively. Insulin resistance was determined using the homeostasis model assessment (HOMA) equation (fasting insulin μU/ml × fasting glucose mg/dl/405) for time 0.

Insulin Tolerance Test

DM mice were injected intraperitoneally with Humulin (0.25 U/kg of body weight) after 3 hours of fasting at the end of IH exposures. Blood was collected from the tail vein of each mouse, and blood glucose was measured using a OneTouch Ultra2 glucometer (LifeScan, Milpitas, CA). Analysis of insulin tolerance test (ITT) glycemic trajectories was conducted as previously described (5).

vWAT Insulin Responses and Immunoblotting Procedures

vWATs were collected from each experimental group. Primary adipocytes were then isolated using first collagenase digestion followed by flotation centrifugation. Cells were then incubated with insulin at 0 or 5 nM at 37°C for 10 minutes with gentle vortexing every 2 minutes as previously described (15). After two washes with cold Krebs–Ringer buffer, adipocytes were lysed in RIPA buffer that was supplemented with a mixture of protease and phosphatase inhibitors (Sigma, St. Louis, MO) and vortexed briefly. The supernatants were then collected after centrifugation at 15,000 × *g* for 15 minutes at 4°C. Protein concentrations were evaluated using the BCA kit (Life Technologies). Equal amounts of total proteins from individual strains were electrophoresed using SDS-PAGE gel (4–20%) and transferred into a nitrocellulose membrane (Millipore, Billerica, MA). After the membrane transfer, incubation in blocking buffer (5% nonfat dry milk in 25 mM Tris, pH 7.4, 3.0 mM KCl, 140 mM NaCl, and 0.05% Tween 20 [TBST]) for 1 hour at room temperature was performed. The membranes were incubated with phospho-Akt (Ser473) antibody (1:1,000, cat. no. 9271S; Cell Signaling Technology, Danvers, MA), total Akt antibody (tAKT, 1:1,000, cat. no. 9272S; Cell Signaling Technology), phosphor eukaryotic initiation factor 2 (eIF2a) α subunit (peIF2a, 1:500, cat. no. 9721; Cell Signaling Technology), total eIF2a (teIF2a, 1:1,000, cat. no. 5324; Cell Signaling Technology), and activating transcription factor 4 (AFT4, 1:500 dilution, cat. no. NB100-852; Novus Biologicals, Littleton, CO) overnight at 4°C. The membranes were then triple washed (10 min each) with TBST and incubated with anti-rabbit IgG and horseradish peroxidase–linked antibody (Cell Signaling Technology) in blocking buffer for 1 hour at room temperature. Immune-reactive bands were subjected to an enhanced chemiluminescence detection assay (Chemidoc XRS+; Bio-Rad; Hercules, CA), and digital images were quantified by Image Lab software (Bio-Rad).

RNA Isolation and Quantitative RT-PCR

Total RNA was isolated from vWAT using automated RNA extraction (Promega, Madison, WI) according to the manufacturer's protocol. The RNA quality and integrity were assessed using the Eukaryote Total RNA Nano 6000 LabChip assay (Agilent Technologies, Santa Clara, CA) on an Agilent 2100 Bioanalyzer. Quantitative RT-PCR (qRT-PCR) gene expression assays (TaqMan; Applied Biosystems, Foster City, CA) were performed using TaqMan gene expression. cDNAs were synthesized from 500 μg of vWAT total RNA using a High-Capacity cDNA Archive Kit (Applied Biosystems) according to the manufacturer's instructions. Gene expression was quantified as the second step of a two-step RT-PCR. Reaction conditions consisted of preincubation at 50°C for 2 minutes and 95°C for 10 minutes, followed by 40 cycles of 95°C for 15 seconds and 60°C for 1 minute. As a reference gene, 18S recombinant RNA was used to normalize the expression ratios. All experiments were performed in triplicate. The mean cycle number (C_t) values of the 18S C_t and the gene of interest C_t were calculated. The relative expression of the gene of interest was calculated by the $2^{-\Delta\Delta Ct}$ method.

Flow Cytometry and vWAT T Regulatory Lymphocyte and Macrophage Characteristics

After incubation with collagenase (1 mg/ml; Worthington Biochemical Corp., Lakewood, NJ) at 37°C for 45 minutes with shaking, vWAT pads were dissociated in Krebs–Ringer buffer supplemented with 1% BSA. The cells were then filtered through a 100-μm mesh and centrifuged at 500 *g* for 5 minutes to separate floating adipocytes and stromal-vascular fraction (SVF) pellets. The SVF pellets were subsequently suspended in fluorescence-activated cell sorting (FACS) buffer (PBS plus 2% FBS). For flow-cytometry analysis, SVF pellets were fixed with 1% paraformaldehyde solution for 30 minutes at 25°C and washed twice. Nonspecific binding was blocked with FcR blocker (1:50; Miltenyi Biotec, San Diego, CA) and then samples were stained with specific antibodies. For surface staining, we used the following fluoro-conjugated antibodies: CD11b-PB, F4/80-PE/Cy7, CD11c-APC, Ly-6c-APC/APC-Cy7, CD206-PE, and CD86-PerCP/Cy5 (BD Biosciences, San Jose, CA). Isotype control antibodies were also used to establish background fluorescence. All antibodies were obtained from BioLegend (San Diego, CA). Data were acquired on a FACS CantoII cytometer using the FACS Diva 5.5 software (BD Biosciences). Analyses were then performed offline using the FlowJo software (Tree Star, Ashland, OR). vWAT macrophages were defined as $F4/80^+$ and $CD11b^+$ cells, and M1 and M2 macrophages were then identified as $CD11c^+$ and $CD206^+$ cells, respectively. Regulatory T cells (Tregs) were identified as $CD3^+$, $CD4^+$, $CD25^{high+}$, and Forkhead box $P3^+$ ($FoxP3^+$), and proinflammatory macrophages that derived from bone marrow were identified as $Ly6c^{high+}$.

Statistical Analysis

All data are reported as mean ± standard deviation. Comparisons of all quantitative data groups were performed using unpaired Student's *t* tests, nonparametric tests, or ANOVA as appropriate. For all comparisons, $P < 0.05$ was considered statistically significant.

Results

Body Weight Changes after IH Exposures

In this study, all three types of knockout mice that were exposed to IH for 6 weeks (DM, $GADD34^{-/-}$, and $PERK^{-/+}$) manifested minor and not statistically significant body weight decreases compared with WT mice, which when exposed to IH underwent significant reductions in body weight (WT-IH: 25.8 ± 1.4 g versus WT-RA: 26.22 ± 2.1 g, $n = 11$/group, $P = 0.008$; DM-IH: 26.8 ± 1.6 g versus DM-RA: 27.4 ± 1.8 g, $n = 20$/group; $P > 0.05$; $PERK^{-/+}$-IH: 24.1 ± 1.1 g versus $PERK^{-/+}$-RA: 24.7 ± 1.3 g; $P > 0.05$, $n = 11$/group; $GADD34^{-/-}$-IH: 23.9 ± 1.8 g versus $GADD34^{-/-}$-RA: 24.5 ± 2.1 g; $P > 0.05$; $n = 10$/group).

IH Exposures and GTT and ITT Responses

During GTTs, significantly higher peak glycemic levels after glucose injection and slower glycemic decline kinetics were apparent in WT-IH mice compared with WT-RA mice (Figure 1A; WT-IH versus WT-RA: $P < 0.001$; $n = 8$/group). For DM mice, no differences in blood glucose levels were observed between mice exposed to IH or RA (Figure 1B, DM-IH versus DM-RA: $P > 0.05$; $n = 8$/group). Two-way ANOVA showed significant two-way interactions of glucose versus × IH ($F = 12.42$, $P < 0.01$) at 10 and 30 minutes.

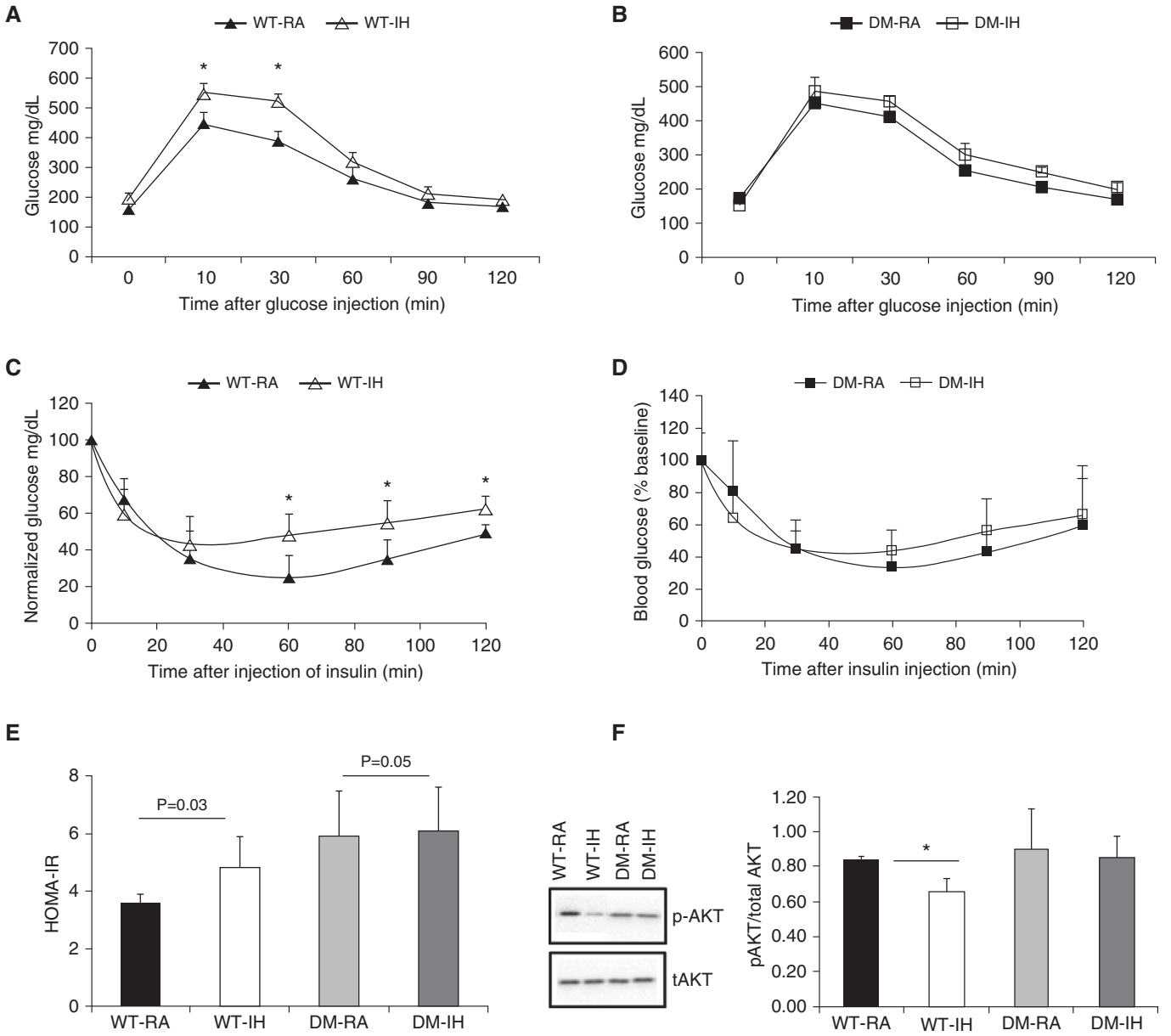

Figure 1. Intraperitoneal glucose tolerance tests (GTTs) and insulin tolerance tests (ITTs). Adult male double-mutant (DM) mice ($CHOP^{-/-}$/$GADD34^{-/-}$) and wild-type (WT) mice were exposed to either intermittent hypoxia (IH) or room air (RA) for 6 weeks. GTTs and ITTs were performed, and fasting homeostatic model assessment insulin resistance (HOMA-IR) was assessed. *A* and *B* illustrate GTT responses for WT and DM mice, and indicate that IH induces abnormal glycemic responses in WT but not in DM mice (two-way ANOVA for repeated measures, $P < 0.001$). *C* and *D* show ITT experimental results, revealing the presence of systemic insulin resistance in WT-IH mice but not in DM-IH mice (two-way ANOVA for repeated measures, $P < 0.001$). Please note that glucose blood levels are shown as % of fasting baseline. (*E*) HOMA-IR values for WT and DM mice: HOMA-IR values were significantly increased in WT-IH mice, whereas such changes were absent in DM-IH mice ($P < 0.01$, DM versus WT). (*F*) Representative Western blot for phosphorylated Akt (p-AKT) and total Akt (tAKT) responses to 5 nM exogenous insulin in visceral white adipose tissue (vWAT) adipocyte lysates from adult male DM mice ($CHOP^{-/-}$/$GADD34^{-/-}$) and WT mice that were exposed to either IH or RA for 6 weeks. *$P < 0.01$; DM versus WT: $P < 0.001$, ANOVA. Data are presented as mean ± SD; n = 8–10/experimental group.

After insulin administration during ITT, WT-IH mice exhibited higher plasma glucose levels, indicating the presence of insulin resistance (WT-IH versus WT-RA: $P < 0.001$; n = 8/group; Figure 1C), whereas no significant differences in insulin-induced glycemic responses were apparent in DM mice (DM-IH versus DM-RA; $P > 0.05$; n = 8/group; Figure 1D). Two-way ANOVA showed significant two-way interactions of glucose × IH (F = 18.12, < 0.002) at 60, 90, and 120 minutes.

Similarly, fasting HOMA-estimated insulin resistance (HOMA-IR) revealed significant increases in the WT-IH group (5.38 ± 1.10) compared with the WT-RA group (3.59 ± 1.25; P = 0.03; n = 8/group; Figure 1E). The HOMA-IR values

calculated for DM-IH mice (5.21 ± 1.19; n = 8/group) were similar to those obtained for DM-RA mice (5.06 ± 1.64; n = 8/group; Figure 1E), and concurred with previous reports of increased baseline HOMA-IR values in $CHOP^{-/-}$ mice (6). For $GADD34^{-/-}$ mice, the HOMA-IR values were similar after IH or RA exposures, and similarly, no significant differences in HOMA-IR were identified in $PERK^{-/+}$-IH mice (1.13 ± 0.11; n = 8/group) compared with $PERK^{-/+}$-RA mice (1.16 ± 0.60; $P > 0.05$). In contrast, $PERK^{+/+}$ mice exposed to IH displayed increased HOMA-IR values (1.73 ± 0.65; n = 8/group) versus $PERK^{+/+}$-RA mice (0.99 ± 0.33; n = 8/group; $P < 0.01$).

vWAT adipocyte insulin sensitivity was assessed by changes in Akt phosphorylation after exogenous insulin administration. p-AKT/total/AKT ratios indicated the presence of increased insulin resistance in WT-IH mice compared with WT-RA. However, were no significant differences in insulin sensitivity with regard to vWAT adipocyte p-AKT/total/AKT ratios in DM-IH mice compared with DM-RA mice (Figure 1F; n = 8 per group).

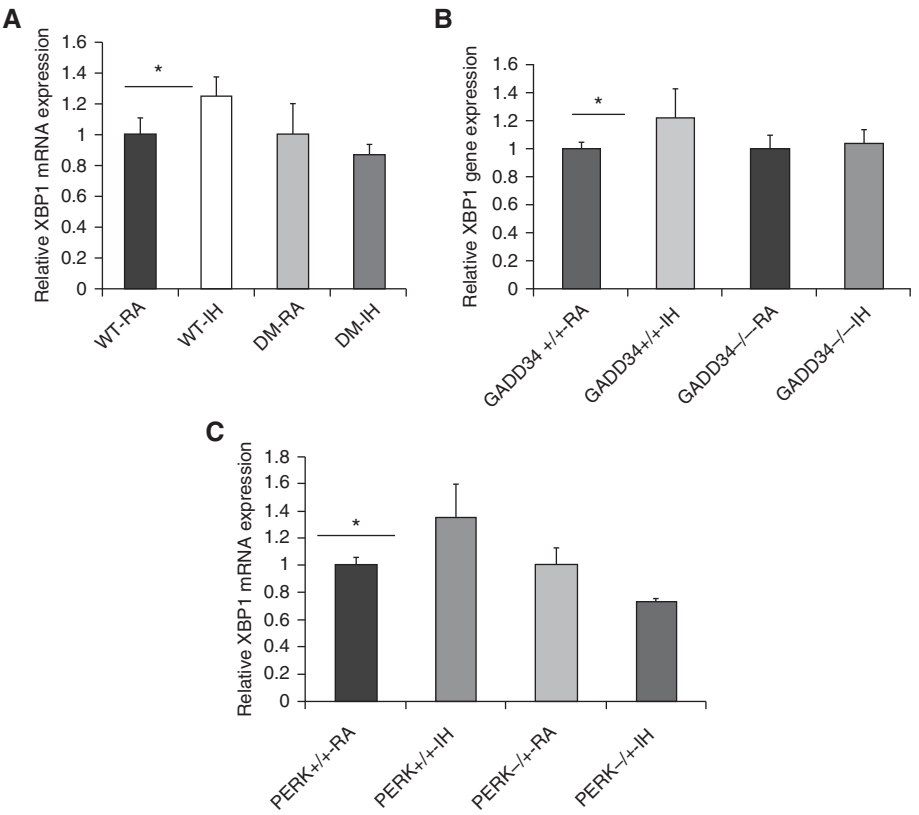

Figure 2. IH induces spliced XBP1 in vWAT. Adult male transgenic mice (DM $CHOP^{-/-}$/$GADD34^{-/-}$ [panel *A*], $GADD34^{-/-}$ [panel *B*], and $PERK^{-/+}$ [panel *C*]) and corresponding WT mice were exposed to IH or RA for 6 weeks. Total RNA was isolated from vWAT and analyzed by qRT-PCR analysis for XBP-1 mRNA expression. qPCR data were normalized to 18 s recombinant RNA as an internal control. Spliced XBP1 expression was increased in all WT mice after IH but not in mutant mice. Data are presented as mean ± SD; n = 8/experimental condition; *$P < 0.02$. PERK, PKR-like endoplasmic reticulum kinase; XBP1, X-box binding protein 1.

ISR

Spliced XBP1 gene expression. To explore the IRE1 signal pathway, we assessed spliced XBP1 expression in the vWAT of all experimental mouse groups exposed to either IH or RA. We observed that the gene expression of spliced XBP1 was significantly increased in WT-IH mice, but not in DM-IH mice (Figure 2A). Similarly, $PERK^{-/+}$-IH and $GADD34^{-/-}$-IH mice did not show increases in spliced XBP1 expression, whereas such increases were apparent in $PERK^{+/+}$-IH and $GADD43^{+/+}$-IH mice compared with RA-exposed mice (Figures 2B and 2C, respectively; n = 8/group).

p-eIF2α and ATF4 Expression

To assess ER stress markers in our animal models, we examined changes in p-eIF2α and ATF4 by Western blotting in vWAT. As shown in Figure 3A, the p-eIF2α/eIF2α ratios were increased in WT-IH (2.61 ± 0.34 versus WT-RA: 0.89 ± 0.03; n = 6/group; P = 0.01), but no changes emerged in DM mice (DM-IH: 1.48 ± 0.34 versus 1.38 ± 0.21; n = 6/group; $P > 0.45$). Similarly, no changes in p-eIF2α/eIF2α ratios occurred in $PERK^{-/+}$-IH compared with $PERK^{-/+}$-RA mice, or in $GADD34^{-/-}$-IH compared with $GADD34^{-/-}$-RA mice, whereas significant increases in p-eIF2α/eIF2α ratios emerged in both $PERK^{+/+}$ and $GADD34^{+/+}$ mice exposed to IH ($P < 0.01$; Table 1).

Expression of ATF4 was significantly increased in WT-IH compared with WT-RA mice (Figure 3B; $P < 0.02$), whereas no significant changes were observed in DM mice (DM-IH versus DM-RA: $P > 0.05$). We also observed statistically significant changes in IH in $PERK^{+/+}$ and $GADD34^{+/+}$, but not in the corresponding IH-exposed heterozygotes or null mice, respectively (Table 1).

Treg Lymphocytes and Macrophages in vWAT

Deregulation of ISR can actively participate in the development and maintenance of pathophysiological states, including metabolic diseases (7, 16–18). In addition, the accumulation of macrophages and changes in their polarity in adipose tissues correlate with increasing body weight and insulin resistance (19). To examine the impact of ISR on IH-induced vWAT inflammation, we evaluated changes in Treg lymphocytes and macrophages from the DM and corresponding WT mice. As anticipated based on previous findings (7), not only were macrophages increased in vWAT from WT-IH mice (29.4 ± 1.0% in IH versus 27.0 ± 0.45% in RA; $P < 0.034$), but their polarity was shifted toward M1, as evidenced by increased M1/M2 ratios (Figures 4A and 4B; $P < 0.01$; n = 8/experimental group). No changes in either the number of macrophages or their polarity emerged in DM mice ($P > 0.05$; n = 8/group). Similarly, in single-gene mutant mice (GADD34 or PERK), increases in M1/M2 ratios occurred in WT mice exposed to IH ($GADD34^{+/+}$-IH versus $GADD34^{+/+}$-RA: P = 0.003; n = 6;

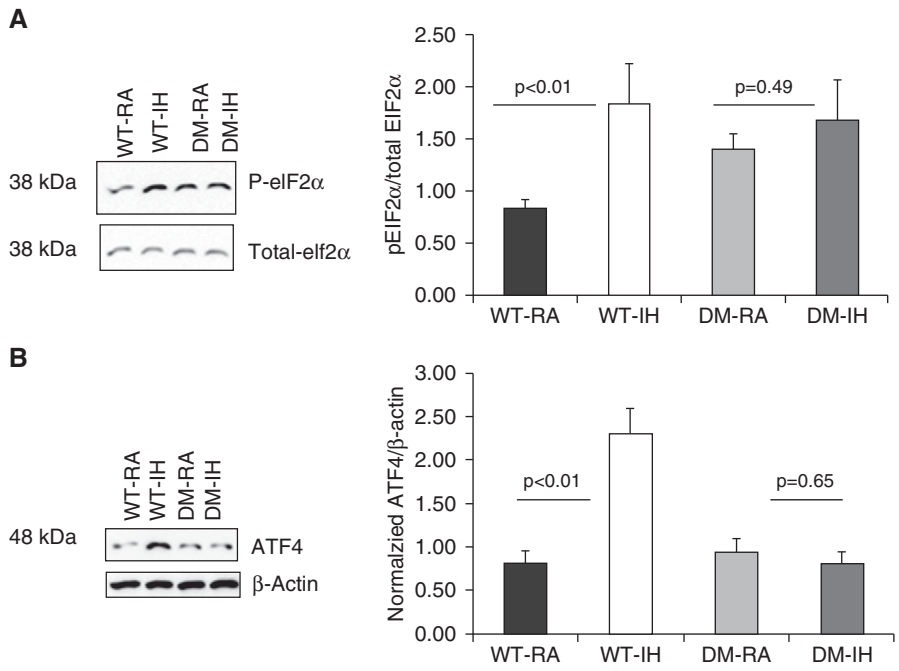

Figure 3. Representative Western blots and quantitative densitometry analyses for eIF2a and ATF4 proteins. DM mice (CHOP$^{-/-}$/GADD34$^{-/-}$) and WT mice were exposed to either IH or RA for 6 weeks. (*A*) eIF2α phosphorylation was increased by IH in WT-IH mice but not in DM-IH mice. Total proteins were isolated from individual vWATs from individual mice and immunoblotted against p-eIF2α and total eIF2α. Representative immunoblots and a summary of signal intensity ratios across experimental groups are shown. (*B*) Representative immunoblot for ATF4 protein and β-actin as the loading control in vWAT, and summary of signal intensities across experimental groups after normalization to β-actin as the loading control. Significant increases in ATF4 expression occurred in WT-IH but not in DM-IH. Results are expressed as fold change and represent mean ± SD, n = 8/experimental group. Data are presented as mean ± SD. ATF4, activating transcription factor 4; eIF2, eukaryotic translation initiation factor 2.

PERK$^{+/+}$-IH versus PERK$^{+/+}$-RA: P = 0.04; n = 5), but no significant changes occurred in GADD34$^{-/-}$ or PERK$^{-/+}$ mice exposed to IH (Table 2). Increases in Ly6c^{high+} cells were observed in WT-IH mice, suggesting an increase in proinflammatory monocyte recruitment from the bone marrow to the vWAT, and such increases were absent in DM-IH mice (P = 0.05; Figures 4C and 4D).

In addition, WT-IH mice showed significant decreases in FoxP3^{+} cells as compared with WT-RA mice, suggesting a decrease in the vWAT Treg lymphocyte population (P = 0.04; Figures 4E and 4F). In contrast, IH did not alter the number or relative proportion of FoxP3^{+} cells in the vWAT of DM mice (Figure 4). Similar findings emerged in single-mutant mice (Table 2).

Discussion

The chronic IH that characterizes OSA is firmly believed to play a predominant role in the pathophysiology of the morbidities associated with this highly prevalent condition, including excessive daytime sleepiness, neurobehavioral deficits, and cardiovascular and metabolic dysfunction (20–25). Several lines of evidence have linked deregulation of the ISR pathway to obesity, insulin resistance, and type 2 diabetes (26–28). Here, we show that chronic IH exposures activated the initiators of UPR signal transduction pathways (namely, PERKeIF2a-ATF4 and IRE1-XBP-1S) in WT mice, and that such IH-induced ISR activation was abrogated in DM mice as well as in single-mutant mice (PERK$^{-/+}$ and GADD34$^{-/-}$). Furthermore, IH not only increased the number of macrophages in vWAT but also shifted their polarity toward a proinflammatory phenotype, as evidenced by both the increases in M1/M2 and the number of Ly-6c^{high+} macrophages, which remained unchanged in DM mice as well as in single-mutant mice exposed to IH. Conversely, FoxP3^{+} Treg lymphocytes were significantly decreased in vWAT of WT-IH mice, but not in DM-IH mice. The functional consequences of such changes were manifest as increases in systemic and vWAT adipocyte insulin resistance in WT-IH, and despite the fact that DM mice exhibited an altered baseline metabolic and inflammatory phenotype, the changes with IH were absent in DM mice. Taken together, our current findings support the concept that sustained and prolonged activation of the ISR by IH mimicking sleep apnea may promote the development of metabolic derangements such as insulin resistance and vWAT inflammation (see Figure 5).

Before we discuss the potential implications of the present study, some methodological aspects deserve comment. First, the IH-exposure paradigm has been extensively used, with slight variations in terms of cycle and daytime duration, and $F_{I_{O_2}}$ nadir. Despite these minor differences, overall, it has been shown that when IH is

Table 1. Western Blot Analyses of ISR in Visceral White Adipose Tissue of GADD34 and PERK Transgenic Mice Exposed to IH and RA

	GADD34$^{+/+}$-RA	GADD34$^{+/+}$-IH	GADD34$^{-/-}$-RA	GADD34$^{-/-}$-IH	PERK$^{+/+}$-RA	PERK$^{+/+}$-IH	PERK$^{-/+}$-RA	PERK$^{-/+}$-IH
p-elf2α/elf2α	0.70 ± 0.05*	1.09 ± 0.08*	0.95 ± 0.1	0.85 ± 0.09	0.42 ± 0.13*	0.68 ± 0.20*	0.44 ± 0.26	0.37 ± 0.28
ATF4	0.84 ± 0.13*	1.13 ± 0.17*	0.91 ± 0.07*	0.58 ± 0.024*	0.59 ± 0.028*	1.09 ± 0.13*	0.50 ± 0.07	0.53 ± 0.15

Definition of abbreviations: ATF4, activating transcription factor 4; IH, intermittent hypoxia; ISR, integrated stress response; PERK, PKR-like endoplasmic reticulum kinase; RA, room air.
*P < 0.05 IH versus RA.

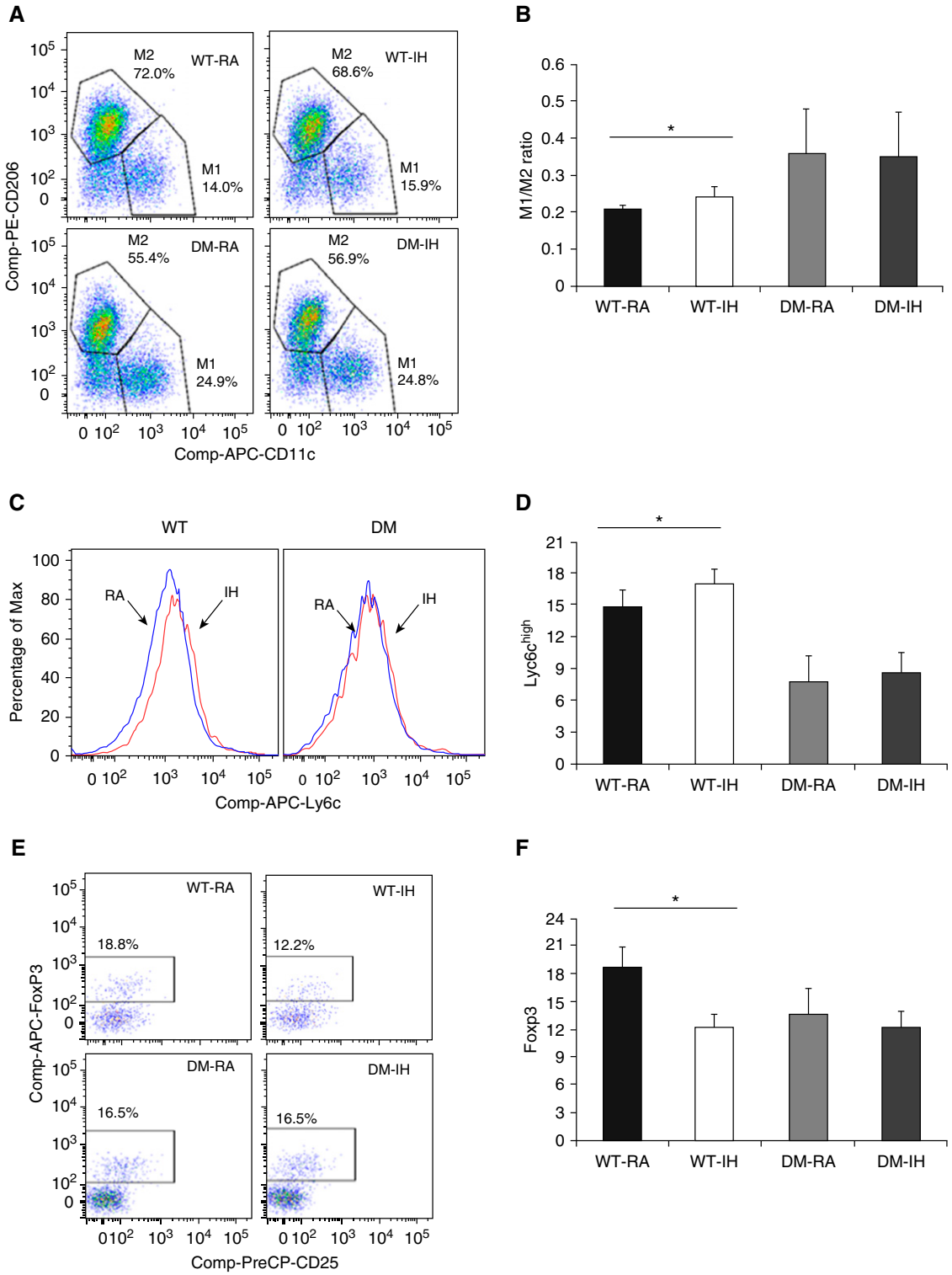

Figure 4. Inflammatory cells in vWAT after IH exposures. Epididymal fat pads were dissected, and stromal-vascular fraction cells were isolated and subjected to FACS analyses. Adipose tissue macrophages were defined as F4/80^{+} and CD11b^{+} cells, from which M1 and M2 macrophages were identified as CD11c^{+} and CD206^{+} cells, respectively. In all of the experiments, macrophages were identified as CD11b-F4/80 double-positive cells. In addition, CD3^{+}, CD4^{+}, CD25^{+}, and FoxP3^{high+} cells were identified as regulatory T lymphocytes (Tregs), and proinflammatory bone-marrow–derived activated macrophages were defined as Ly6c^{high+} cells. (*A* and *B*) Example of flow-cytometry analysis for M1 and M2, and summary of M1/M2 ratios across all four experimental groups. (*C* and *D*) Representative example of Ly6c^{high+} proinflammatory macrophage flow cytometry and group summary. (*E* and *F*) Representative example of Treg flow cytometry and summary of findings from the four experimental groups. Data are presented as mean ± SD (n = 8/experimental group). *$P < 0.01$.

Table 2. Flow-Cytometry Analyses of Treg Lymphocytes and Macrophages in Visceral White Adipose Tissue of GADD34 and PERK Transgenic Mice Exposed to IH and RA

	GADD34$^{+/+}$-RA	GADD34$^{+/+}$-IH	GADD34$^{-/-}$-RA	GADD34$^{-/-}$-IH	PERK$^{+/+}$-RA	PERK$^{+/+}$-IH	PERK$^{-/+}$-RA	PERK$^{-/+}$-IH
M1 (%)	19.4 ± 2.6*	22.6 ± 3.9*	21.8 ± 3.8	20.6 ± 2.7	15.29 ± 2.66*	19.36 ± 2.16*	18.33 ± 2.49	18.11 ± 2.06
M2 (%)	65.2 ± 3.6	63.5 ± 2.5	65.2 ± 2.5	66.1 ± 3.4	71.13 ± 3.04*	68.21 ± 2.57*	68.87 ± 3.20	67.96 ± 3.51
M1/M2 ratio	0.27 ± 0.0*	0.32 ± 0.04*	0.30 ± 0.01	0.28 ± 0.02	0.32 ± 0.03*	0.41 ± 0.02*	0.40 ± 0.04	0.42 ± 0.02
Foxp3^{+} (%CD3^{+})	22.5 ± 11.95*	17.93 ± 2.30*	13.69 ± 2.44	13.80 ± 3.54	17.9 ± 1.81*	13.8 ± 0.61*	14.17 ± 0.93	14.33 ± 0.94
Ly6c MFI	1,095 ± 118*	1,238 ± 36.4*	1,080 ± 150	1,110 ± 117.01	1,012 ± 40*	1,315 ± 43.80*	833.11 ± 52.85	908.05 ± 75.23

Definition of abbreviations: IH, intermittent hypoxia; MFI, mean fluorescent intensity; PERK, PKR-like endoplasmic reticulum kinase; RA, room air.
*$P < 0.05$ IH versus RA.

applied for prolonged periods of time (spanning weeks to months), it induces adverse metabolic consequences, such as hyperlipidemia and insulin resistance, even in lean C57BL/6J mice, along with structural and cellular remodeling of adipose and vascular tissues (22, 29–31). Such tissue remodeling appears to be mediated by oxidative stress and downstream activation of inflammation (32), which appears to involve ISR-related pathways (9). However, the mechanistic role of sustained ISR in the deleterious metabolic consequences of OSA has not been investigated, and the current work provides novel and important insights into this issue. Second, in addition to examining systemic changes in glucose disposition as reporters of insulin sensitivity changes, we also explored vWAT adipocytes to further highlight the role of the ISR in cellular tissue substrates. Third, we systematically assessed three types of transgenic mice in which different aspects of the ISR were targeted. Thus, the consistency of the responses to IH across all three murine models further reinforces the assumption that the ISR plays a critical role in chronic IH. Finally, we noticed a trend toward increased body weight and HOMA-IR in normoxic DM mice. In this regard, a higher body and vWAT mass have been previously reported in both CHOP and GADD34 (33) single-deletion mutant mice. However, despite the higher vWAT mass, CHOP$^{-/-}$ mice did not show evidence of insulin resistance. In addition, the impact of GADD34 deletion on glucose metabolism was recently investigated at different time points in the natural life span (7), and GADD34$^{-/-}$ mice exhibit higher insulin sensitivity until the age of 3 months, which could participate in the process of vWAT accretion (33). As such, considering the alterations in adipose tissue mass and increased risk for developing insulin resistance, the absence of IH-induced changes in insulin sensitivity or inflammatory cell characteristics in the mutant mice needs to be viewed with caution, since some of the underlying baseline abnormalities could mask the IH response. However, considering that high-fat diets and obesity are highly prevalent among patients with OSA, it might be of interest to pursue studies on the role of ISR in experimental models in which diet and IH are examined concurrently.

The evidence pointing to an important role of the ISR in metabolic homeostasis is not novel. Indeed, activation of the ISR has been implicated in the pathogenesis of obesity and diabetes in both hepatic and white adipose tissues (34, 35). The ER plays critical roles in a wide range of processes, including *1*) synthesis, folding, modification, and transport of proteins; *2*) synthesis and distribution of phospholipids and steroids; and *3*) storage of calcium ions (36). Perturbations of any of these functions can result in misfolded or unfolded proteins, which then accumulate in the ER until they are properly folded or destroyed (37). In general, when the ER is overwhelmed by the accumulation of misfolded or unfolded proteins (i.e., ER stress), the ISR is activated and the expression of chaperones is upregulated to help fold the ER proteins (38, 39). Dysregulation of ER integrity as induced by a high-fat diet can actively participate in the development and maintenance of metabolic diseases (40). However, we are unaware of any studies examining the role of long-term ISR activation in IH-induced insulin resistance and vWAT inflammation.

In our study, we preferentially used DM mice (CHOP$^{-/-}$/GADD34$^{-/-}$) to more extensively target and encompass the chronic ISR pathway activation by IH, and thus better explore its role in IH-induced changes in insulin sensitivity within vWAT. Our findings indicate that DM mice may be protected from IH-induced metabolic and proinflammatory effects, even though definitive conclusions cannot be drawn regarding the underlying baseline metabolic alterations that develop in these mice. CHOP and GADD34 can activate downstream PERK homodimerization and autophosphorylation during chronic ISR activation. CHOP is a bZIP transcription factor whose expression is strongly induced by ER stress, and it also acts as a proapoptotic transcription factor. It has been shown that the PERK pathway is necessary for upregulating CHOP expression, and PERK activation may reflect the attenuation of translation through phosphorylation of eIF2α, whereas protein folding and the degradation capacity increase (41). On the other hand, GADD34 is a stress-inducible regulatory subunit of a phosphatase complex that is known to dephosphorylate p-eIF2α, thereby allowing recovery from the global suppression of protein synthesis. Overexpression of a constitutively active form of GADD34 that dephosphorylates eIF2α attenuates eIF2α phosphorylation and severely inhibits ATF4 induction. This suggests that GADD34 functions as an important negative-feedback regulator of the PERK signaling pathway (42). Thus, DM mice would not only maintain the protective phosphorylated state of eIF2α but also mitigate the effects of CHOP, thereby playing an extensive and protective role in chronic IH conditions. Surprisingly, even mice with single mutations of ISR-related genes (i.e., PERK$^{-/+}$ or GADD34$^{-/-}$) were also protected from IH-induced metabolic and proinflammatory consequences, a finding that further supports the potential role of chronic ISR activation in IH.

The visceral adipose tissue depot is a central player in metabolic regulation through the production and release of multiple adipokines, and extensive crosstalk with other organs and tissues (43, 44). In this context, chronic low-grade inflammation in adipose tissues is a key process for the emergence of insulin resistance (45, 46), and hypoxia can

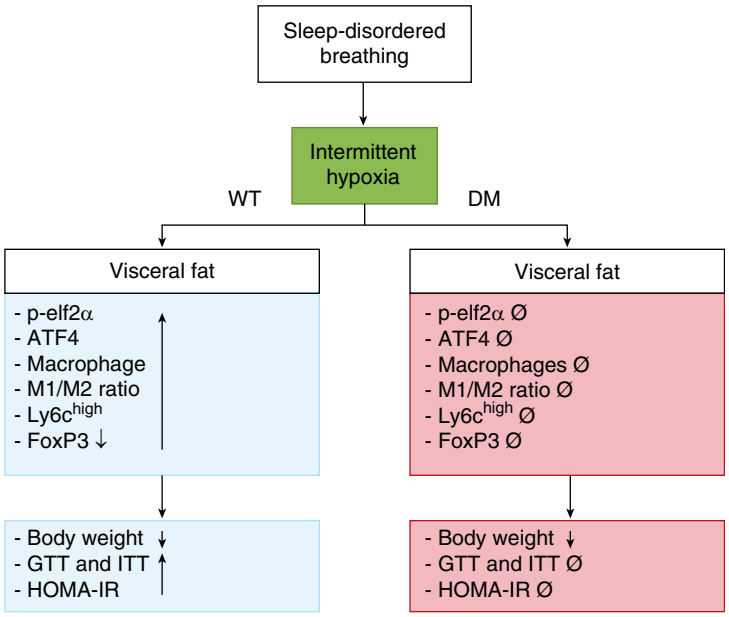

Figure 5. Schematic diagram illustrating the effects of intermittent hypoxia on metabolic function using both WT and DM knockout mice.

amplify this phenomenon via recruitment and polarization of macrophages within the vWAT (47). Furthermore, adipocytes and inflammatory cells, such as macrophages, show a high degree of interaction in obesity (43). Thus, the reduced capacity of the adipose tissues to preserve their homeostatic function in obesity is caused by impairment of key cellular functions, among which is included ISR deregulation in adipocytes (48). Indeed, sustained ISR activation is mechanistically implicated in adipose tissue inflammation and insulin resistance in various settings, including aging, obesity, and high-fat diet, and interventions aimed at reducing the ISR have resulted in either prevention of metabolic dysfunction or restoration of insulin sensitivity (49, 50).

In the current study, we explored evidence pointing to activation of the ISR by IH using multiple approaches. At the mRNA level, splicing of XBP1 mRNA (8) has been implicated in obesity-induced insulin resistance and type 2 diabetes (9–11). When ER stress occurs, IRE1a promotes alternative XBP-1 mRNA processing, involving the removal of a 26-nucleotide intron. This process results in the production of spliced XBP-1 (XBP-1 s), which is a powerful gene transactivation factor, particularly relative to lipogenic genes. In the current experiments, IH induced increased XBP-1 s expression in WT-IH mice, but this was prevented in mutant mice. Since eIF2α phosphorylation contributes to the reduced formation of translational preinitiation complexes and activates the translation of ATF4, which accumulates under stress and activates CHOP expression (51), we assessed both events and uncovered their enhanced presence in WT-IH mice, but not in the targeted mutant mice.

In WT-IH mice, we found an increase in the global number of macrophages detected in the SVF and a decrease in Treg lymphocytes. IH-induced changes in both M1 macrophages and Treg lymphocytes were conspicuously absent in DM mice exposed to IH. However, we should point out that the normoxic DM mice already exhibited fewer proinflammatory macrophages despite having higher M1/M2 ratios, even if such ratios do not change in IH, indicating that the genotype effect is robust and may restrict our ability to draw definitive conclusions regarding the role of IH-induced ISR in macrophage polarity. Taken together, these findings suggest that vWAT inflammation likely contributed to the insulin resistance in WT-IH mice.

Conclusions

As shown in Figure 5, physiological and pathological conditions can disrupt ER homeostasis, resulting in an accumulation of misfolded and unfolded proteins. This study shows that the ISR is potentially involved in insulin resistance and vWAT inflammation induced by long-term IH mimicking OSA. ■

Author disclosures are available with the text of this article at www.atsjournals.org.

References

1. Iurlaro R, Muñoz-Pinedo C. Cell death induced by endoplasmic reticulum stress. *FEBS J* 2016;283:2640–2652.
2. Kent BD, McNicholas WT, Ryan S. Insulin resistance, glucose intolerance and diabetes mellitus in obstructive sleep apnoea. *J Thorac Dis* 2015;7:1343–1357.
3. Drager LF, Polotsky VY, O'Donnell CP, Cravo SL, Lorenzi-Filho G, Machado BH. Translational approaches to understanding metabolic dysfunction and cardiovascular consequences of obstructive sleep apnea. *Am J Physiol Heart Circ Physiol* 2015;309:H1101–H1111.
4. Gileles-Hillel A, Kheirandish-Gozal L, Gozal D. Biological plausibility linking sleep apnoea and metabolic dysfunction. *Nat Rev Endocrinol* 2016;12:290–298.
5. Wang Y, Carreras A, Lee S, Hakim F, Zhang SX, Nair D, Ye H, Gozal D. Chronic sleep fragmentation promotes obesity in young adult mice. *Obesity (Silver Spring)* 2014;22:758–762.
6. Ryan S. Adipose tissue inflammation by intermittent hypoxia: mechanistic link between obstructive sleep apnoea and metabolic dysfunction. *J Physiol* 2017;595:2423–2430.
7. Carreras A, Zhang SX, Almendros I, Wang Y, Peris E, Qiao Z, Gozal D. Resveratrol attenuates intermittent hypoxia-induced macrophage migration to visceral white adipose tissue and insulin resistance in male mice. *Endocrinology* 2015;156:437–443.
8. Hakim F, Wang Y, Carreras A, Hirotsu C, Zhang J, Peris E, Gozal D. Chronic sleep fragmentation during the sleep period induces hypothalamic endoplasmic reticulum stress and PTP1b-mediated leptin resistance in male mice. *Sleep* 2015;38:31–40.
9. Belaidi E, Thomas A, Bourdier G, Moulin S, Lemarié E, Levy P, Pépin JL, Korichneva I, Godin-Ribuot D, Arnaud C. Endoplasmic reticulum stress as a novel inducer of hypoxia inducible factor-1 activity: its role in the susceptibility to myocardial ischemia-reperfusion induced by chronic intermittent hypoxia. *Int J Cardiol* 2016;210:45–53.
10. Cnop M, Foufelle F, Velloso LA. Endoplasmic reticulum stress, obesity and diabetes. *Trends Mol Med* 2012;18:59–68.
11. Marciniak SJ, Yun CY, Oyadomari S, Novoa I, Zhang Y, Jungreis R, Nagata K, Harding HP, Ron D. CHOP induces death by promoting protein synthesis and oxidation in the stressed endoplasmic reticulum. *Genes Dev* 2004;18:3066–3077.

12. Kojima E, Takeuchi A, Haneda M, Yagi A, Hasegawa T, Yamaki K, Takeda K, Akira S, Shimokata K, Isobe K. The function of GADD34 is a recovery from a shutoff of protein synthesis induced by ER stress: elucidation by GADD34-deficient mice. *FASEB J* 2003;17: 1573–1575.
13. Harding HP, Zeng H, Zhang Y, Jungries R, Chung P, Plesken H, Sabatini DD, Ron D. Diabetes mellitus and exocrine pancreatic dysfunction in perk-/- mice reveals a role for translational control in secretory cell survival. *Mol Cell* 2001;7:1153–1163.
14. Gileles-Hillel A, Almendros I, Khalyfa A, Zhang SX, Wang Y, Gozal D. Early intermittent hypoxia induces proatherogenic changes in aortic wall macrophages in a murine model of obstructive sleep apnea. *Am J Respir Crit Care Med* 2014;190:958–961.
15. Gozal D, Qiao Z, Almendros I, Zheng J, Khalyfa A, Shimpukade B, Ulven T. Treatment with TUG891, a free fatty acid receptor 4 agonist, restores adipose tissue metabolic dysfunction following chronic sleep fragmentation in mice. *Int J Obes* 2016;40: 1143–1149.
16. Ozcan L, Tabas I. Calcium signalling and ER stress in insulin resistance and atherosclerosis. *J Intern Med* 2016;280:457–464.
17. Safiedeen Z, Andriantsitohaina R, Martinez MC. Dialogue between endoplasmic reticulum and mitochondria as a key actor of vascular dysfunction associated to metabolic disorders. *Int J Biochem Cell Biol* 2016;77(Pt A):10–14.
18. Maris M, Overbergh L, Gysemans C, Waget A, Cardozo AK, Verdrengh E, Cunha JP, Gotoh T, Cnop M, Eizirik DL, *et al*. Deletion of C/EBP homologous protein (Chop) in C57Bl/6 mice dissociates obesity from insulin resistance. *Diabetologia* 2012;55:1167–1178.
19. Xu H, Barnes GT, Yang Q, Tan G, Yang D, Chou CJ, Sole J, Nichols A, Ross JS, Tartaglia LA, *et al*. Chronic inflammation in fat plays a crucial role in the development of obesity-related insulin resistance. *J Clin Invest* 2003;112:1821–1830.
20. Gharib SA, Khalyfa A, Abdelkarim A, Ramesh V, Buazza M, Kaushal N, Bhushan B, Gozal D. Intermittent hypoxia activates temporally coordinated transcriptional programs in visceral adipose tissue. *J Mol Med (Berl)* 2012;90:435–445.
21. Gozal D, Capdevila OS, Kheirandish-Gozal L. Metabolic alterations and systemic inflammation in obstructive sleep apnea among nonobese and obese prepubertal children. *Am J Respir Crit Care Med* 2008; 177:1142–1149.
22. Guest JF, Panca M, Sladkevicius E, Taheri S, Stradling J. Clinical outcomes and cost-effectiveness of continuous positive airway pressure to manage obstructive sleep apnea in patients with type 2 diabetes in the U.K. *Diabetes Care* 2014;37: 1263–1271.
23. Koren D, Dumin M, Gozal D. Role of sleep quality in the metabolic syndrome. *Diabetes Metab Syndr Obes* 2016;9:281–310.
24. Lavie L. Oxidative stress in obstructive sleep apnea and intermittent hypoxia—revisited—the bad ugly and good: implications to the heart and brain. *Sleep Med Rev* 2015;20:27–45.
25. Mokhlesi B, Ham SA, Gozal D. The effect of sex and age on the comorbidity burden of OSA: an observational analysis from a large nationwide US health claims database. *Eur Respir J* 2016;47: 1162–1169.
26. Ozcan U, Yilmaz E, Ozcan L, Furuhashi M, Vaillancourt E, Smith RO, Görgün CZ, Hotamisligil GS. Chemical chaperones reduce ER stress and restore glucose homeostasis in a mouse model of type 2 diabetes. *Science* 2006;313:1137–1140.
27. Leonard A, Paton AW, El-Quadi M, Paton JC, Fazal F. Preconditioning with endoplasmic reticulum stress ameliorates endothelial cell inflammation. *PLoS One* 2014;9:e110949.
28. Meares GP, Liu Y, Rajbhandari R, Qin H, Nozell SE, Mobley JA, Corbett JA, Benveniste EN. PERK-dependent activation of JAK1 and STAT3 contributes to endoplasmic reticulum stress-induced inflammation. *Mol Cell Biol* 2014;34:3911–3925.
29. Drager LF, Li J, Shin MK, Reinke C, Aggarwal NR, Jun JC, Bevans-Fonti S, Sztalryd C, O'Byrne SM, Kroupa O, *et al*. Intermittent hypoxia inhibits clearance of triglyceride-rich lipoproteins and inactivates adipose lipoprotein lipase in a mouse model of sleep apnoea. *Eur Heart J* 2012;33:783–790.
30. Badran M, Golbidi S, Devlin A, Ayas N, Laher I. Chronic intermittent hypoxia causes endothelial dysfunction in a mouse model of diet-induced obesity. *Sleep Med* 2014;15:596–602.
31. Drager LF, Li J, Reinke C, Bevans-Fonti S, Jun JC, Polotsky VY. Intermittent hypoxia exacerbates metabolic effects of diet-induced obesity. *Obesity (Silver Spring)* 2011;19:2167–2174.
32. Zhou S, Yin X, Zheng Y, Miao X, Feng W, Cai J, Cai L. Metallothionein prevents intermittent hypoxia-induced cardiac endoplasmic reticulum stress and cell death likely via activation of Akt signaling pathway in mice. *Toxicol Lett* 2014;227:113–123.
33. Nishio N, Isobe K. GADD34-deficient mice develop obesity, nonalcoholic fatty liver disease, hepatic carcinoma and insulin resistance. *Sci Rep* 2015;5:13519.
34. Flamment M, Kammoun HL, Hainault I, Ferré P, Foufelle F. Endoplasmic reticulum stress: a new actor in the development of hepatic steatosis. *Curr Opin Lipidol* 2010;21:239–246.
35. Schröder M. Endoplasmic reticulum stress responses. *Cell Mol Life Sci* 2008;65:862–894.
36. Rutkowski DT, Kaufman RJ. That which does not kill me makes me stronger: adapting to chronic ER stress. *Trends Biochem Sci* 2007; 32:469–476.
37. Zhang K, Kaufman RJ. From endoplasmic-reticulum stress to the inflammatory response. *Nature* 2008;454:455–462.
38. Scheuner D, Song B, McEwen E, Liu C, Laybutt R, Gillespie P, Saunders T, Bonner-Weir S, Kaufman RJ. Translational control is required for the unfolded protein response and in vivo glucose homeostasis. *Mol Cell* 2001;7:1165–1176.
39. Ron D, Walter P. Signal integration in the endoplasmic reticulum unfolded protein response. *Nat Rev Mol Cell Biol* 2007;8:519–529.
40. Blais JD, Filipenko V, Bi M, Harding HP, Ron D, Koumenis C, Wouters BG, Bell JC. Activating transcription factor 4 is translationally regulated by hypoxic stress. *Mol Cell Biol* 2004;24: 7469–7482.
41. Trayhurn P, Wood IS. Adipokines: inflammation and the pleiotropic role of white adipose tissue. *Br J Nutr* 2004;92:347–355.
42. Lee DE, Kehlenbrink S, Lee H, Hawkins M, Yudkin JS. Getting the message across: mechanisms of physiological cross talk by adipose tissue. *Am J Physiol Endocrinol Metab* 2009;296: E1210–E1229.
43. Wensveen FM, Valentić S, Šestan M, Turk Wensveen T, Polić B. The "big bang" in obese fat: events initiating obesity-induced adipose tissue inflammation. *Eur J Immunol* 2015;45:2446–2456.
44. Cho KW, Zamarron BF, Muir LA, Singer K, Porsche CE, DelProposto JB, Geletka L, Meyer KA, O'Rourke RW, Lumeng CN. Adipose tissue dendritic cells are independent contributors to obesity-induced inflammation and insulin resistance. *J Immunol* 2016;197: 3650–3661.
45. Fujisaka S, Usui I, Ikutani M, Aminuddin A, Takikawa A, Tsuneyama K, Mahmood A, Goda N, Nagai Y, Takatsu K, *et al*. Adipose tissue hypoxia induces inflammatory M1 polarity of macrophages in an HIF-1α-dependent and HIF-1α-independent manner in obese mice. *Diabetologia* 2013;56:1403–1412.
46. Wang L, Zhang B, Huang F, Liu B, Xie Y. Curcumin inhibits lipolysis via suppression of ER stress in adipose tissue and prevents hepatic insulin resistance. *J Lipid Res* 2016;57:1243–1255.
47. Burrill JS, Long EK, Reilly B, Deng Y, Armitage IM, Scherer PE, Bernlohr DA. Inflammation and ER stress regulate branched-chain amino acid uptake and metabolism in adipocytes. *Mol Endocrinol* 2015;29: 411–420.
48. Ghosh AK, Garg SK, Mau T, O'Brien M, Liu J, Yung R. Elevated endoplasmic reticulum stress response contributes to adipose tissue inflammation in aging. *J Gerontol A Biol Sci Med Sci* 2015;70: 1320–1329.
49. Sriburi R, Jackowski S, Mori K, Brewer JW. XBP1: a link between the unfolded protein response, lipid biosynthesis, and biogenesis of the endoplasmic reticulum. *J Cell Biol* 2004;167:35–41.
50. Lee AH, Glimcher LH. Intersection of the unfolded protein response and hepatic lipid metabolism. *Cell Mol Life Sci* 2009;66:2835–2850.
51. Harding HP, Novoa I, Zhang Y, Zeng H, Wek R, Schapira M, Ron D. Regulated translation initiation controls stress-induced gene expression in mammalian cells. *Mol Cell* 2000;6:1099–1108.